Next Materials 12 (2026) 102277

Contents lists available at ScienceDirect

Next Materials

journal homepage: www.sciencedirect.com/journal/next-materials

Research article

Valorization of shrimp waste into a thermally modified biosorbent for the removal of cationic and anionic dyes

Soumia El Boumlasy [a,c,d,*,1], Iman Kouda [a,b,2], Mohamed Achache [a,**,3], Federico La Spada [c,4], Nunzio Tuccitto [d,5], Santa Olga Cacciola [c,6], Abderrahmane Debdoubi [a]

[a] Laboratory of Engineering Materials and Sustainable Energy (LEMSE), Faculty of Science, Abdelmalek Essaadi University, BP 2121, Tetouan 93002, Morocco
[b] Separation Processes Laboratory, Department of Chemistry, Faculty of Sciences, Ibn Tofail University, Kenitra, Morocco
[c] Department of Agriculture, Food and Environment, University of Catania, Catania, Italy
[d] Department of Chemical Sciences, University of Catania, Catania, Italy

ARTICLE INFO

Keywords:
Adsorption
Biosorbent
Methyl orange
Methylene blue
Thermal treatment
Shrimp-waste powder

ABSTRACT

Shrimp waste powder (SWP) and its mildly thermally treated derivative obtained at 200 °C in air (TT-SWP) were investigated as low-cost biosorbents for the removal of methylene blue (MB) and methyl orange (MO) from aqueous solution. The aim was to determine whether a simple reagent-free thermal treatment could improve the adsorption behavior of raw SW without harsh activation procedures. SWP and TT-SWP were characterized by SEM, EDX, FTIR, XRD, and ζ-potential analysis, and their adsorption performance was evaluated as a function of sorbent dose, pH, contact time, initial dye concentration, and temperature. Thermal treatment modified the surface morphology and near-surface properties of the material, producing a rougher and more fissured surface and improving adsorption behavior, particularly for MO. Adsorption was strongly pH-dependent, with MB favored at neutral to alkaline pH and MO under acidic conditions. Kinetic data were best described by the pseudo-second-order model, whereas equilibrium data were most consistently fitted by the Langmuir model, supporting a predominantly monolayer adsorption regime with limited heterogeneity. At 298 K, the Langmuir maximum adsorption capacities were 101.02 and 115.05 mg g^{-1} for SWP toward MB and MO, respectively, and 94.18 and 123.85 mg g^{-1} for TT-SWP. Thermodynamic analysis indicated endothermic MB adsorption and exothermic MO adsorption, with relatively low enthalpy values supporting adsorption dominated by physical interactions. Desorption and regeneration tests showed feasible reuse of both sorbents, although with progressive performance loss over repeated cycles. These findings support mild thermal treatment as a simple upgrading strategy for SW derived sorbents.

1. Introduction

Industrial effluents, especially from the textile, paper, leather, and printing industries, contribute significantly to environmental pollution, impacting both ecosystems and human health [1]. These wastewaters frequently contain high loads of synthetic dyes; global dye production exceeds 700,000 t yr^{-1} , and an estimated 10–15% is discharged with effluents during dyeing operations [2–4]. Representative dyes, namely MB and MO, are environmentally problematic due to their resistance to degradation and their toxic effects on both aquatic organisms and

* Correspondence to: Laboratory of Materials Engineering and Sustainable Energy, Faculty of Science, Abdelmalek Essaadi University, BP 2121, Tetouan 93002, Morocco.
** Corresponding author.
E-mail addresses: soumia.elboumlasy@unict.it (S. El Boumlasy), iman.kouda@uit.ac.ma (I. Kouda), mohamed.achache@etu.uae.ac.ma (M. Achache), federico.laspada@unict.it (F.L. Spada), n.tuccitto@unict.it (N. Tuccitto), olga.cacciola@unict.it (S.O. Cacciola), adebdoubi@uae.ac.ma (A. Debdoubi).
[1] 0000-0003-3970-8420
[2] 0009-0004-1324-7202
[3] 0009-0007-4153-3371
[4] 0000-0002-0911-3998
[5] 0000-0003-4129-0406
[6] 0000-0001-7926-3601

https://doi.org/10.1016/j.nxmate.2026.102277
Received 5 May 2026; Accepted 12 May 2026
Available online 19 May 2026

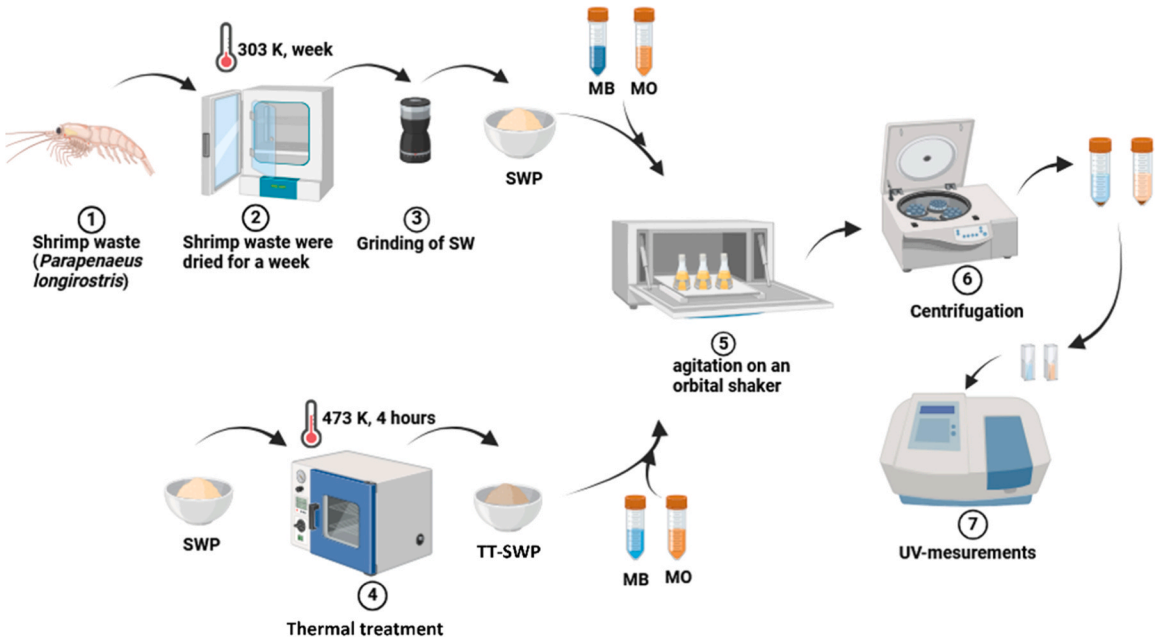

Scheme 1. Preparation of SWP and TT-SWP.

human health [5–8]. Growing pressure on freshwater resources driven by climate change and population growth further underscores the need for effective, affordable dye-removal technologies [2]. Within this context, adsorption remains one of the most widely investigated treatment strategies because of its operational simplicity, flexibility, and comparatively low-cost relative to coagulation-flocculation, advanced oxidation, and membrane-based processes, which may involve high energy demand, higher operating costs, or the generation of secondary sludge [9].

A broad spectrum of adsorbents has been investigated for dye removal, including activated carbons, polymeric resins, mineral clays, biochars, and more recently developed porous materials, with performance depending on textural properties, surface chemistry, and affinity toward the target pollutant. In recent years, increasing attention has been directed toward low-cost biosorbents derived from agricultural, forestry, and food-processing residues, in line with waste-valorization and circular-economy strategies [7,10–13]. This growing interest reflects the recognition that abundant biowastes may provide accessible adsorption sites through their natural content of oxygenated, nitrogen-containing, and mineral functional domains, while also reducing disposal burdens associated with agro-industrial residues [14].

Among these materials, shrimp-processing residues are particularly attractive because the shrimp industry generates large amounts of shells, heads, and tails, which can create disposal and environmental management problems if not properly handled [8,15,16]; SW is a naturally heterogeneous matrix mainly composed of chitin, proteins, and calcium carbonate, together with minor lipidic and pigment fractions, and this compositional complexity makes it a potentially versatile precursor for sorbent development [17]. Accordingly, shrimp-derived materials have been widely studied in different forms, especially chitin, chitosan, and chemically modified shell-based adsorbents. However, despite this substantial body of work, the direct use of SWP itself, and particularly its thermally treated form, remains much less explored than more extensively processed derivatives. This gap is relevant from both scientific and practical perspectives. Compared with chemical modification routes, simple thermal treatment may offer several potential advantages, including a more straightforward preparation procedure, the avoidance of additional chemical reagents, reduced generation of secondary liquid waste, and potentially lower processing cost. At the same time, even mild heating may significantly alter surface morphology, accessibility of adsorption sites, the distribution of organic and mineral surface domains, and the acid-base or interfacial properties of the material. Therefore, thermally treated shrimp waste powder (TT-SWP) may represent an attractive intermediate between untreated biowaste and heavily modified shrimp-derived sorbents, combining process simplicity with potentially improved adsorption performance [8,12,18,19]. Another limitation in the available literature is that many studies focus either on a single dye system or on strongly processed shrimp-derived materials, making it difficult to isolate the specific effect of mild thermal treatment on adsorption behavior. In particular, direct comparisons between untreated SWP and its mildly thermally treated counterpart toward dyes of opposite charge remain limited. Such a comparison is relevant not only for evaluating adsorption efficiency, but also for clarifying how low-severity thermal treatment affects structure-property-performance relationships in a heterogeneous chitin-calcite-based sorbent.

On this basis, the originality of the present study lies in the comparative evaluation of raw SWP and its mildly thermally treated derivative obtained at 200 °C in air (TT-SWP) as low-cost biosorbents for the removal of both MB and MO from aqueous solution. The novelty does not reside solely in testing a SW derived adsorbent, but in specifically examining whether a simple and reagent-free thermal treatment can modify morphology, surface chemistry, and charge behavior sufficiently to improve adsorption performance, while retaining the practical advantages of a low-cost and scalable preparation route. To address this objective, SWP and TT-SWP were characterized by scanning electron microscopy coupled with energy-dispersive X-ray spectroscopy (SEM/EDX), Fourier transform infrared spectroscopy (FTIR), X-ray diffraction (XRD), and zeta-potential (ζ-E) measurements, and their adsorption behavior was evaluated through batch experiments as a function of adsorbent dosage, pH, initial dye concentration, contact time, and temperature. By combining physicochemical characterization with adsorption, kinetic, isotherm, and thermodynamic analyses, the present work aims to clarify the dye-dependent effects of mild thermal treatment and to assess the potential of SW derived sorbents for sustainable water-treatment applications.

Table 1
Process parameters and their levels.

Parameter	Level 1	Level 2	Level 3	Level 4	Level 5	Level 6
pH	2	4	7	9	-	-
Initial concentration (mg L^{-1})	50	100	200	300	400	500
Contact time (min)	10	30	60	120	240	360
Adsorbent Dose (mg)	100	200	300	400	600	800
Temperature (K)	298	308	318	-	-	-

2. Experimental section

2.1. Reagents and apparatus

MO ($C_{14}H_{14}N_3NaO_3S$), MB ($C_{16}H_{18}ClN_3S$), sodium hydroxide (NaOH, ≥99.9%), and hydrochloric acid (HCl, 37%) were purchased from Sigma-Aldrich (St. Louis, USA) and used as received. Distilled water (DW) was used for all solution preparations and washing steps. UV-Vis spectra were recorded with a PerkinElmer Lambda 25 using 1 cm quartz cuvettes at λ_{max} = 664–665 nm (MB) and 465 nm (MO). Solution pH was adjusted with standardized NaOH and HCl solutions and verified with a calibrated pH meter.

2.2. Preparation of sorbents

Shrimp processing waste (cephalothorax, head, and carapace) from Parapenaeus longirostris (deep-water pink shrimp) was collected from a local fish market in Tetouan (Morocco) and transported to the laboratory on ice. The material was washed with DW, drained, and dried in an oven at 303 K for 3 days, until a constant mass was achieved [20]. The dried waste was then ground and sieved to a particle size of ≤ 250 μm to obtain the SWP. For thermal treatment, SWP was heated in an oven at 473 K for 4 h in air and subsequently cooled to room temperature to produce the TT-SWP. The temperature of 473 K was selected as a mild thermal-treatment condition to induce physicochemical modification of the shrimp-shell-derived material while avoiding extensive degradation of its main constituents. This choice is consistent with literature on the thermal behavior of shrimp-shell biomass and chitin-rich materials, which shows that lower-temperature mass loss is mainly associated with moisture removal, whereas the main decomposition of the organic fraction becomes more pronounced at higher temperatures, while calcium carbonate remains stable until much higher temperatures. Both SWP and TT-SWP were stored in airtight containers in a desiccator until use. No additional chemical or physical activation was applied prior to the adsorption experiments (see Scheme 1).

2.3. Characterizations

SEM was performed on a Nova NanoSEM 450 (FEI, Hillsboro, OR, USA) to examine the surface morphology of SWP and TT-SWP. Powders were mounted on aluminum stubs using double-sided carbon tape. FTIR spectra were acquired on a PerkinElmer Spectrum 2000 equipped with an ATR accessory from 4500 to 500 cm^{-1}, at a resolution of 4 cm^{-1} with 16 co-added scans. XRD patterns were collected on a Bruker D8 ADVANCE using Cu K_α radiation (λ = 1.5418 Å) operated at 40 kV and 25 mA. Data were recorded over 2θ = 5–65° and processed with High-Score Plus software. Surface charge was evaluated by ζ-E measurements. For each adsorbent, 0.10 g was dispersed in 50 mL of deionized water, and the pH was adjusted from 2 to 11 using 0.1 M HCl or 0.1 M NaOH. After 360 min of agitation at room temperature on a rotary shaker, the final pH was recorded and the ζ-E was determined using a Zetasizer Nano instrument (Malvern Panalytical, UK).

2.4. Adsorption experiments

Batch equilibrium adsorption of MB and MO onto SWP and TT-SWP was evaluated. The effects of adsorbent dosage, pH, temperature, contact time, and initial dye concentration were investigated (Table 1). Stock solutions of MB and MO (1000 mg L^{-1}) were prepared in deionized water and diluted as required. For all experiments, 25 mL aliquots containing the desired adsorbent mass were transferred into 100 mL Erlenmeyer flasks. The solutions were adjusted to the target pH using 0.1 M NaOH or 0.1 M HCl and shaken at 150 rpm for 360 min at ambient temperature. Equilibrium dye concentrations were determined using a UV-Vis spectrophotometer (PerkinElmer Lambda 25) at 664 nm for MB and 465 nm for MO. All batch adsorption experiments were performed in triplicate, and the results are reported as mean ± standard deviation. Error bars shown in the figures represent the standard deviation of three independent replicates (n = 3). For isotherm analysis, non-linear regressions were weighted by replicate standard deviations. The equilibrium adsorption capacity (q_e) and the percentage of dye removal were determined using Eqs. (1) and (2) [21]:

$$q_e = \frac{(C_0 - C_e)V}{m} \tag{1}$$

$$\%\ \ Adsorption = \frac{(C_o - C_e)}{C_o} \times 100 \tag{2}$$

where $C_0$and C_e(mg L^{-1}) are the initial and equilibrium dye concentrations, V(L) is the solution volume, and m(g) is the mass of adsorbent.

2.5. Adsorption kinetics and adsorption isotherms

Adsorption kinetics describes the time-dependence of uptake (rate, approach to equilibrium, and possible mass-transfer contributions) [22]. Kinetic data for SWP and TT-SWP were fitted with the PFO and PSO models using non-linear regression. The PFO model for solid–liquid systems are expressed in non-linear form by Eq. (3) [23]:

$$q_t = q_e(1 - e^{-k_1 t}) \tag{3}$$

where q_t and q_e(mg g^{-1}) are the amounts adsorbed at time t and at equilibrium, respectively, and k_1 is the PFO rate constant (min^{-1}).

The PSO model is commonly used when the apparent rate depends on the sorbent capacity; although often associated with chemisorption, mechanistic assignments should not rely on goodness-of-fit alone. Its non-linear form is given by Eq. (4):

$$q_t = \frac{K_2 q_e^2 t}{1 + K_2 q_e t} \tag{4}$$

where K_2 is the PSO rate constant (g mg^{-1} min^{-1}).

Adsorption isotherms describe the distribution of solute between solid and liquid phases at equilibrium. Several models can interpret these interactions [24]. In this study, the Langmuir, Freundlich, and Sips models were used.

The Langmuir model assumes energetically equivalent sites and no lateral interactions [25]. The non-linear form used is Eq. (5):

$$q_e = \frac{Q_m K_L C_e}{1 + K_L C_e} \tag{5}$$

where Q_m(mg g^{-1}) is the monolayer capacity, K_L(L mg^{-1}) is the affinity constant, and C_e(mg L^{-1}) is the equilibrium concentration.

The Freundlich model, suitable for heterogeneous surfaces and/or multilayer adsorption [26], is expressed by Eq. (6):

$$q_e = K_F C_e^{\frac{1}{n}} \tag{6}$$

where K_F is the capacity constant [mg g^{-1} (L mg^{-1})$^{1/n_F}$] and 1/n repre-

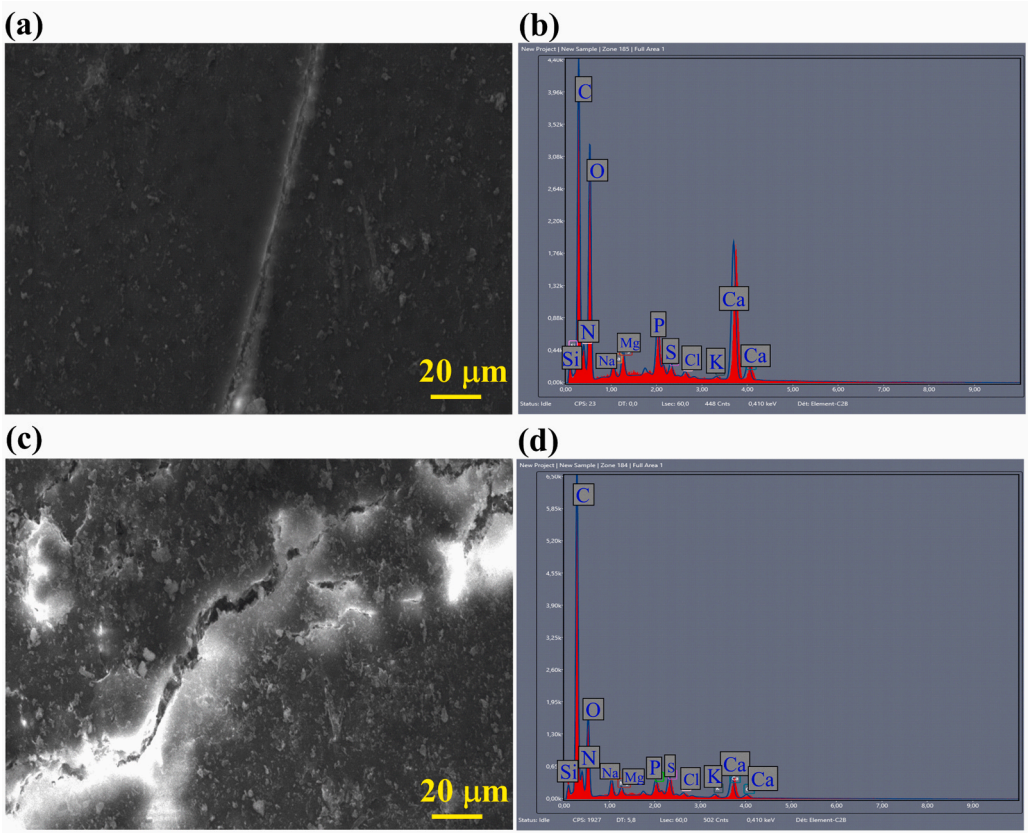

Fig. 1. SEM images of (a) SWP and (c) TT-SWP, and EDX spectra of (b) SWP and (d) TT-SWP.

Table 2
Elemental composition of SWP and TT-SWP as determined by EDX.

Sample name	C wt%	N wt%	O wt%	Na wt%	Mg wt%	Si wt%	P wt%	S wt%	Cl wt%	K wt%	Ca wt%
SWP	25.88	7.45	33.6	1.37	1.61	0.39	3.74	2.99	0.61	0.35	23.88
TT-SWP	49.90	11.12	21.96	2.46	0.87	0.39	2.15	1.13	0.65	0.8	6.6

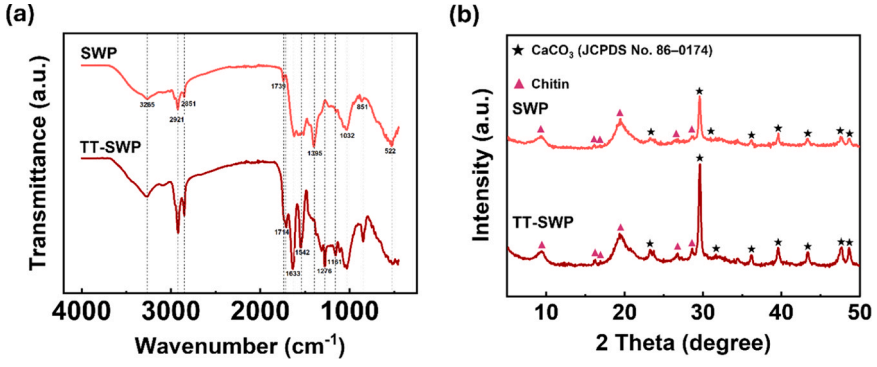

Fig. 2. (a) FTIR spectra; (b) XRD patterns of SWP and TT-SWP.

sents adsorption intensity. Because non-linear regression is used, no logarithmic linearization was applied.

The Sips (Langmuir-Freundlich) model combines Freundlich heterogeneity with Langmuir saturation and is appropriate for non-uniform surfaces [23]. The non-linear form used is Eq. (7):

$$q_e = \frac{Q_m (K_S C_e)^n}{1 + (K_S C_e)^n} \quad (7)$$

where n quantifies system heterogeneity and K_S has units $(\mathrm{L\,mg^{-1}})^n$ to keep q_e in mg $\mathrm{g^{-1}}$.

3. Results and discussion

3.1. Characterizations

3.1.1. SEM and EDX analysis

SEM images of SWP (Fig. 1a) and TT-SWP (Fig. 1c) reveal marked

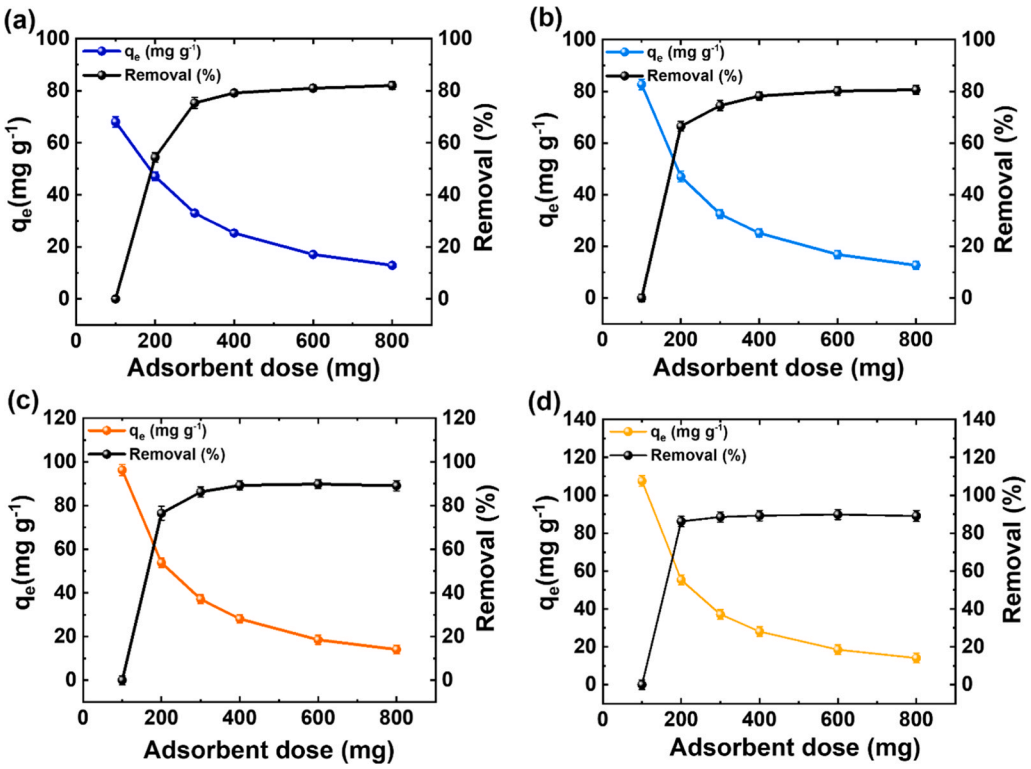

Fig. 3. Effects of sorbent dose on adsorption: (a) SWP–MB, (b) TT-SWP–MB, (c) SWP–MO, (d) TT-SWP–MO (C_0 = 500 mg L^{-1}; V_o = 25 mL; pH = 7; T = 298 K; t = 360 min). Error bars show standard deviation (n = 3).

changes in surface morphology after thermal treatment. SWP shows a comparatively smooth surface, whereas TT-SWP exhibits a rougher texture with abundant small pores and larger fissures. These features are consistent with partial removal and rearrangement of organic matter during heating.

EDX spectra (Fig. 1b and d; Table 2) indicate a relative increase in carbon and nitrogen and a decrease in oxygen for TT-SWP, consistent with near-surface deoxygenation and alteration of surface functionalities; a modest apparent enrichment in sulfur may also be present. Given the surface-sensitive, semiquantitative nature of EDX, these variations are interpreted as near-surface compositional changes rather than precise bulk values. Other inorganic elements (Na, Mg, Si, P, Cl, K, Ca) show lower weight percentages after treatment, which may reflect a combination of surface redistribution, partial removal of loosely bound residues, and matrix effects on EDX quantification rather than wholesale loss of the corresponding bulk phases. Overall, the elemental trends corroborate the SEM observations and indicate that thermal treatment substantially modifies both the surface texture and the near-surface composition of the SWP, enriching carbon and depleting oxygen at the surface, changes relevant to subsequent dye-adsorption performance. As discussed further in the FTIR section, these changes are consistent not only with partial oxygen loss, but also with chemical transformation and redistribution of oxygen-containing surface functionalities.

3.1.2. FTIR and XRD analysis

The FTIR spectra of SWP and TT-SWP (Fig. 2a) display the expected features of a chitin–calcite composite, with clear changes after thermal treatment. A broad band at ~3265 cm^{-1} is assigned to O–H/N–H stretching. Bands at 2921 and 2851 cm^{-1} arise from aliphatic C-H stretching of -CH_2/-CH_3 groups [27–30]. Signals at ~1739 and ~1633 cm-1 are attributable to carbonyl (C═O) stretching and H-O-H bending (with possible overlap from amide I), respectively [28,30]. The band at ~1542 cm^{-1} is characteristic of amide II vibrations of chitin/protein residues [31]. Features near ~1161 and ~1032 cm^{-1} are assigned to C-O-C bridge and C-O stretching typical of polysaccharides [32,33]. A band in the 870–850 cm^{-1} region is consistent with the out-of-plane ν_2 mode of carbonate in $CaCO_3$. After thermal treatment, bands appear/-intensify at ~1714 and ~1276 cm^{-1}, consistent with oxygenated surface groups formed during heating (non-conjugated C═O and C-O stretching, respectively) [34–36]. In parallel, a reduction of aliphatic C-H bending intensity is observed in the 1460–1370 cm^{-1} region, indicating loss/modification of labile aliphatic moieties with temperature [37]. Overall, the spectral changes indicate that thermal treatment does not simply cause partial oxygen loss, but also promotes chemical transformation and redistribution of oxygen-containing organic functionalities, in agreement with the EDX results.

The powder XRD patterns of SWP and TT-SWP (Fig. 2b) are characteristic of calcite ($CaCO_3$; JCPDS 86–0174) [15]. The most intense reflection at 2θ ≈ 29.4° (104) is accompanied by the expected calcite lines at ~23.0° (012), 36.0° (110), 39.4° (113), 43.1° (202), 47.5° (018), and 48.5° (116) (stars). Superimposed on this mineral background, broad low-intensity features attributable to α-chitin are visible at ~9–10° (often assigned to the (020)/(021) family) and ~19–21° ((110)) (triangles). As XRD primarily probes crystalline material, the amorphous organic fraction is not represented in the diffractograms.

The TT-SWP pattern closely matches that of SWP, indicating preservation of the calcite phase under the 473 K (200 °C) treatment. No reflections assignable to CaO (~37.3°, 53.9°) or $Ca(OH)_2$ (~34.1°, 47.1°) are detected within the instrument's limits, consistent with the thermal stability of CaCO3 at this temperature. Compared with SWP, TT-SWP exhibits slightly higher relative intensities of calcite peaks and marginal peak sharpening, consistent with removal of amorphous organics and an increased diffracting volume fraction of the mineral phase rather than mineral recrystallization. The chitin-associated broad bands remain present but appear weaker relative to calcite after treatment, again consistent with a lower amorphous contribution and/or partial disordering of polysaccharide domains during heating.

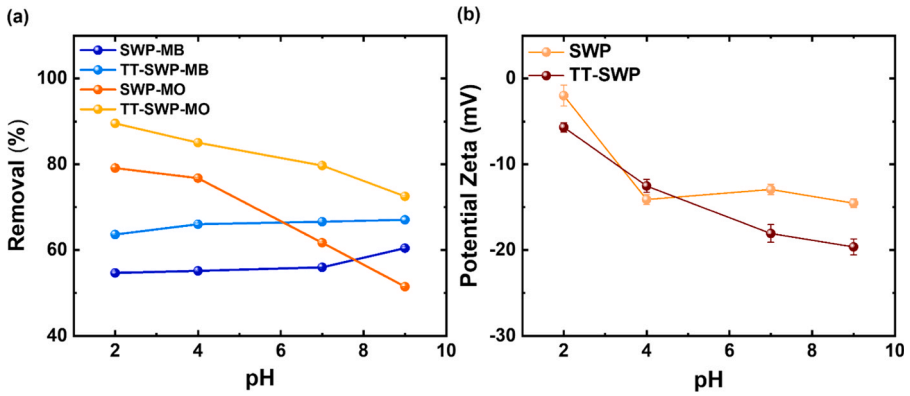

Fig. 4. (a) Effect of pH on MB and MO adsorption onto SWP and TT-SWP; (b) ζ-E measurements (S/L = 4 g L^{-1}; C_o = 500 mg L^{-1}; V_o = 25 mL; pH = 2–9; T = 298 K; t = 360 min). Error bars show standard deviation (n = 3).

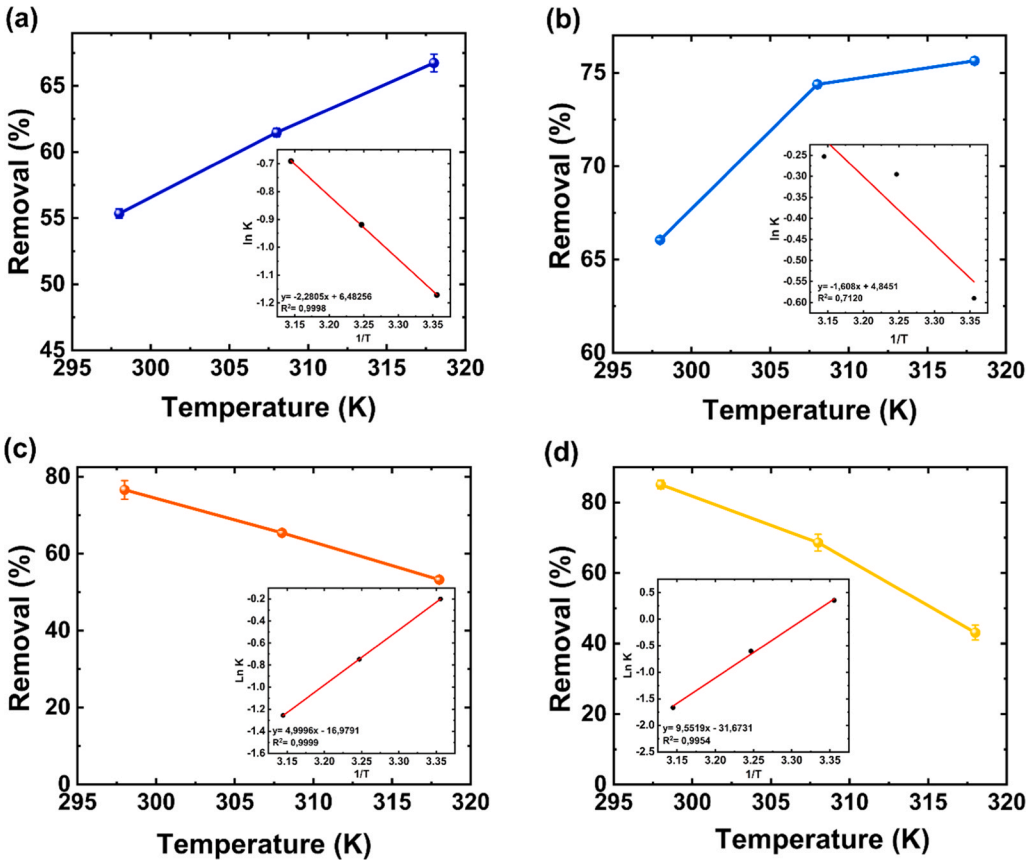

Fig. 5. Effect of temperature on removal efficiency for (a) SWP–MB, (b) TT-SWP–MB, (c) SWP–MO, (d) TT-SWP-MO (S/L = 4 g L^{-1}; C_0 = 500 mg L^{-1}; pH = 7; T = 298–318 K; t = 360 min). Error bars show standard deviation (n = 3).

3.2. Adsorption studies

3.2.1. Effect of adsorbent dose

Fig. 3 illustrates the effects of varying adsorbent dosage, ranging from 10 to 80 mg, on the removal percentages of MB and MO. Notably, an impressive enhancement in the removal percentages of MB and MO by SWP was observed, surging from 54.39% to 82.63%, and from 76.40% to 90.25%, correspondingly, as the mass of the adsorbent escalated from 10 to 40 mg. Analogously, concerning the removal percentages of MB and MO through TT-SWP, substantial increments were detected, progressing from 66.43% to 80.82%, and from 86.21% to 90.25%, respectively, within the 10–40 mg adsorbent mass range. This elevation in removal percentages can be attributed to the heightened availability of adsorption sites, resulting from the increased adsorbent dosage. Consequently, this allowed for more profound interactions with dye molecules, as expounded by [38,39]. The removal percentages began to reach a plateau at 40 mg for both dyes on both adsorbents. This phenomenon could be ascribed to the saturation of binding sites on the surface and/or the limited presence of adsorbate molecules [40]. A significant reduction in adsorption capacities for both dyes on both materials was observed. This trend stems from the persisting unoccupied sites subsequent to the adsorption of MB and MO molecules. Comparing the two adsorbents, TT-SWP demonstrated higher initial removal efficiencies for both MB and MO. Specifically, TT-SWP achieved 66.43% removal for MB and 86.21% for MO, while SWP started at 54.39% for MB and 76.40% for MO. The enhanced performance of TT-SWP can be

Table 3
Thermodynamic parameters for MB and MO reduction onto SWP and TT-SWP adsorbents.

Parameter	ΔH° (KJ mol^{-1})	ΔS° (J mol^{-1} K^{-1})	ΔG° (KJ mol^{-1})		
Temperature (K)			298	308	318
SWP-MB	18.9601	53.8963	2.9022	2.3535	1.8247
TT-SWP-MB	13.3689	40.2822	1.4610	0.7562	0.6688
SWP-MO	-41.5675	-141.1634	0,4985	1,91456	3,3217
TT-SWP-MO	-79.4145	-263.3293	-0,8756	1.5485	4.4002

attributed to its pretreatment process, which likely increases the number of available adsorption sites and improves interactions with dye molecules. Despite both adsorbents reaching a plateau at an adsorbent mass of 40 mg, TT-SWP consistently outperformed SWP across the dosage range. This suggests that TT-SWP, with its superior q_e, could be more effective for applications requiring higher dye removal efficiency.

3.2.2. pH effects on MB and MO adsorption and ζ-E

The pH of the solution plays a pivotal role in governing the q_e, affecting not only the surface charge of the adsorbents but also the solubility of dyes [41]. In this study, the effect of pH on the removal of MB and MO was evaluated (Fig. 4a). For SWP, MB removal increased slightly as pH went from 7 to 9, with the highest removal at pH 9 due to the electrostatic attraction between the negatively charged adsorbent surface and the cationic MB dye. Similarly, TT-SWP showed higher MB removal across all pH values, with an increase in removal from 63.64% to 67.05% as the pH rose from 2 to 9, following a similar trend as SWP [39]. For MO, the removal percentage decreased as pH increased from 2

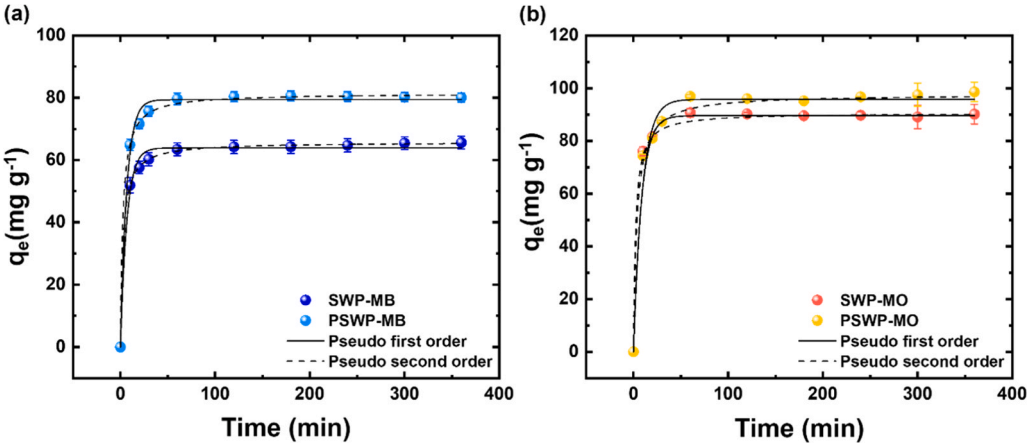

Fig. 6. Experimental adsorption kinetics and non-linear fits to the PFO and PSO models for (a) MB and (b) MO on SWP and TT-SWP (S/L = 4 g L^{-1}; C_o = 500 mg L^{-1}; pH = 7; T = 298 K). Error bars show standard deviation (n = 3).

Table 4
Kinetic parameters for the removal of MB and MO onto SWP and TT-SWP.

Samples	q_e (mg g^{-1})	PFO kinetics			PSO kinetics		
		K_1 (min^{-1})	q_e (mg g^{-1})	R^2	K_2 (g mg^{-1}min^{-1})	q_e (mg g^{-1})	R^2
SWP-MB	65.58	0.14760	63.90	0.99501	0.005602	65.76	0.99694
TT-SWP-MB	80.11	0.15200	79.40	0.99715	0.004847	81.47	0.99804
SWP-MO	90.15	0.12190	89.56	0.98266	0.005057	90.66	0.99389
TT-SWP-MO	98.61	0.10840	95.78	0.99573	0.002802	97.77	0.99867

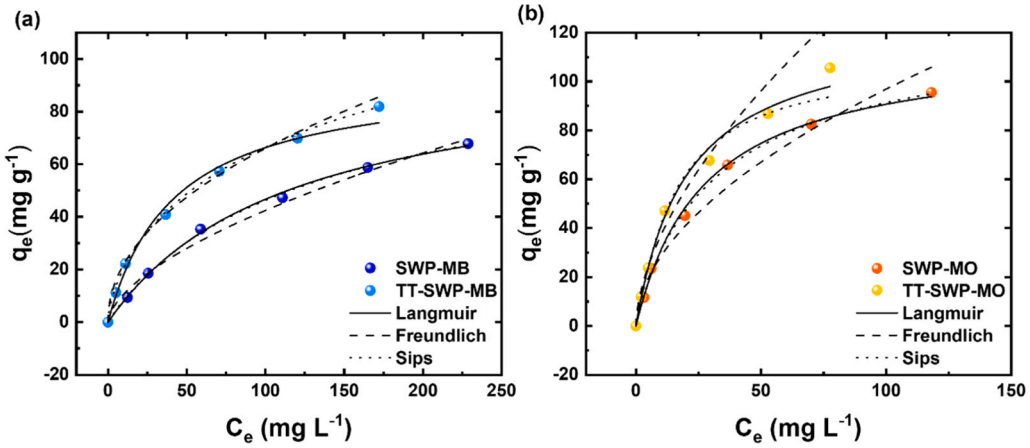

Fig. 7. Experimental adsorption isotherms and non-linear fits to the Langmuir, Freundlich, and Sips models for (a) MB and (b) MO on SWP and TT-SWP (S/L = 4 g L^{-1}; C_o = 10–300 mg L^{-1}; pH = 7; t = 360 min; T = 298 K). Error bars show standard deviation (n = 3).

Table 5
Parameters of different isotherm models for MB and MO adsorption by SWP and TT-SWP.

Isotherm models	Samples	Parameters	Values
	SWP-MB	Q_m (mg g^{-1})	101.02
		k_L (L mg^{-1})	0.0086
		R^2	0.9973
Langmuir	SWP-MO	Q_m (mg g^{-1})	115.05
		k_L (L mg^{-1})	0.0366
		R^2	0.9964
	TT-SWP-MB	Q_m (mg g^{-1})	94.18
		k_L (L mg^{-1})	0.0238
		R^2	0.9843
	TT-SWP-MO	Q_m (mg g^{-1})	123.85
		k_L (L mg^{-1})	0.0488
		R^2	0.9852
	SWP-MB	k_F (mg g^{-1}) (L $mg^{-1})^{1/n}$	2.6888
		1/n	0.5993
		R^2	0.9858
Freundlich	SWP-MO	k_F (mg g^{-1}) (L $mg^{-1})^{1/n}$	8.3749
		1/n	0.5316
		R^2	0.9580
	TT-SWP-MB	k_F (mg g^{-1}) (L $mg^{-1})^{1/n}$)	7.3436
		1/n	0.4765
		R^2	0.9891
	TT-SWP-MO	k_F (mg g^{-1}) (L $mg^{-1})^{1/n}$)	9.4710
		1/n	0.5924
		R^2	0.9117
	SWP-MB	Q_m (mg g^{-1})	108.96
		k_s (L mg^{-1})	0.0073
		n	0.9480
		R^2	0.9976
Sips	SWP-MO	Q_m (mg g^{-1})	124.98
		k_s (L mg^{-1})	0.0295
		n	0.9244
		R^2	0.9979
	TT-SWP-MB	Q_m (mg g^{-1})	177.06
		k_s (L mg^{-1})	0.0046
		n	0.6589
		R^2	0.9972
	TT-SWP-MO	Q_m (mg g^{-1})	110.94
		k_s (L mg^{-1})	0.0632
		n	1.0996
		R^2	0.9738

to 9, with peak removal at pH 2 on both SWP and TT-SWP. The thermal treatment effect was evident on TT-SWP, with higher MO removal observed at lower pH values and better overall removal efficiency compared to SWP [4]. Additionally, ζ-E measurements (Fig. 4**b**) revealed different behaviors for SWP and TT-SWP, highlighting how composition affects surface charge and electrostatic interactions. SWP exhibited a shift towards more negative values as pH increased, while TT-SWP consistently showed more negative ζ-E values, reflecting its enhanced surface charge density from thermal treatment. These results confirm the correlation between pH, surface charge, and pollutant removal efficiency for both adsorbents [42,43].

3.2.3. Temperature effect and thermodynamic study

This study investigated the effect of temperature on the adsorption of MB and MO onto SWP and TT-SWP at 298, 308, and 318 K. As shown in Fig. 5, the removal efficiency of MB increased with temperature, from 55.35% to 66.73% for SWP and from 66.05% to 75.64% for TT-SWP. This behavior indicates that MB adsorption was favored at higher temperatures, consistent with an endothermic process. In contrast, MO removal decreased with increasing temperature, from 76.59% to 53.24% for SWP and from 85.07% to 43.10% for TT-SWP, indicating that MO adsorption became less favorable as temperature increased. This opposite trend is consistent with an exothermic adsorption process, in which increasing thermal energy weakens the interactions responsible for dye uptake [44].

Thermodynamic analysis was performed to evaluate the energetic characteristics and temperature dependence of the adsorption process. The thermodynamic parameters, namely standard Gibbs free energy (ΔG°), enthalpy change (ΔH°), and entropy change (ΔS°), were estimated using the following relationships [45]:

Where, R is the universal gas constant (8.314 J K^{-1} mol^{-1}), T is an absolute temperature (K) and K_d is the equilibrium distribution coefficient.

$$\Delta G^\circ = -RT\ln K_d \tag{8}$$

$$\ln K_d = -\frac{\Delta H^\circ}{RT} + \frac{\Delta S^\circ}{R} \tag{9}$$

ΔG° values were calculated using Eq. (8), while ΔH° and ΔS° were estimated using Eq. (9) from the slope and intercept of the van't Hoff plot, respectively, as illustrated in Fig. 5. The corresponding thermodynamic parameters are presented in Table 3. Positive ΔH° values for MB adsorption on both SWP and TT-SWP indicate that this process was endothermic, in agreement with the observed increase in adsorption with temperature. In contrast, negative ΔH° values for MO adsorption on both sorbents confirm the exothermic nature of this process, consistent with the decrease in removal efficiency at higher temperature [46]. The ΔG° values indicate that the thermodynamic favorability of adsorption depends on both dye type and temperature. For MB, ΔG° decreased with increasing temperature, indicating that adsorption became more favorable at higher temperature. For MO, ΔG° increased with temperature for both sorbents, indicating that adsorption became less favorable as temperature rose. A slightly negative ΔG° was observed only for TT-SWP-MO at 298 K, whereas positive values were obtained at higher temperatures. The relatively low absolute values of ΔH° support the predominance of physical interactions in the adsorption process. In addition, positive values of ΔS° for MB reflect the affinity of the adsorbent towards the adsorbate species. In addition, the positive ΔS° values obtained for MB suggest an increase in randomness at the solid-solution interface during adsorption, which may reflect favorable rearrangement of interfacial species. By contrast, the negative ΔS° values observed for MO indicate a decrease in interfacial randomness and suggest that adsorption proceeded through a more ordered interfacial state. This behavior is also consistent with the exothermic nature of MO adsorption and with the decrease in adsorption capacity as temperature increased [47].

3.2.4. Adsorption kinetics

Adsorption of MB and MO on SWP and TT-SWP increases rapidly at short contact times and approaches equilibrium within ~60 min for all systems. The initial surge reflects the abundance of accessible surface sites, whereas progressive site occupation diminishes the driving force and yields a plateau. Non-linear fits of the pseudo-first-order (PFO) and pseudo-second-order (PSO) models (Fig. 6**a–b**) capture these trends, and the corresponding parameters are summarized in Table 4.

Across all four systems, the PSO model shows the closest agreement with the kinetic data, with higher R^2 values (≈0.994–0.999) and smaller residuals than the PFO model. PFO fits yield positive rate constants ($k_1 \approx$ 0.108–0.152 min^{-1}), indicating that the model is mathematically admissible but empirically inferior for these data. Overall, these results indicate that MB and MO uptake on SWP and TT-SWP follow a PSO-type rate law under the conditions studied.

3.2.5. Adsorption isotherms

The equilibrium uptake of MB and MO increases with $C_e$and approaches a plateau for all sorbent–dye pairs, consistent with progressive occupation of a finite population of sites (Fig. 7). Non-linear regressions (weighted by replicate standard deviations) indicate that the Langmuir model provides the most accurate description across systems (highest $R^2 \approx 0.984$–0.998), while Sips yields comparably good fits and Freundlich tends to deviate at higher C_e, especially for MO. The Langmuir capacities in Table 5 mirror the trends in the plots: $Q_m \approx 101$ and 115mg g^{-1} for SWP with MB and MO, and ≈ 94 and 124 mg g^{-1} for TT-

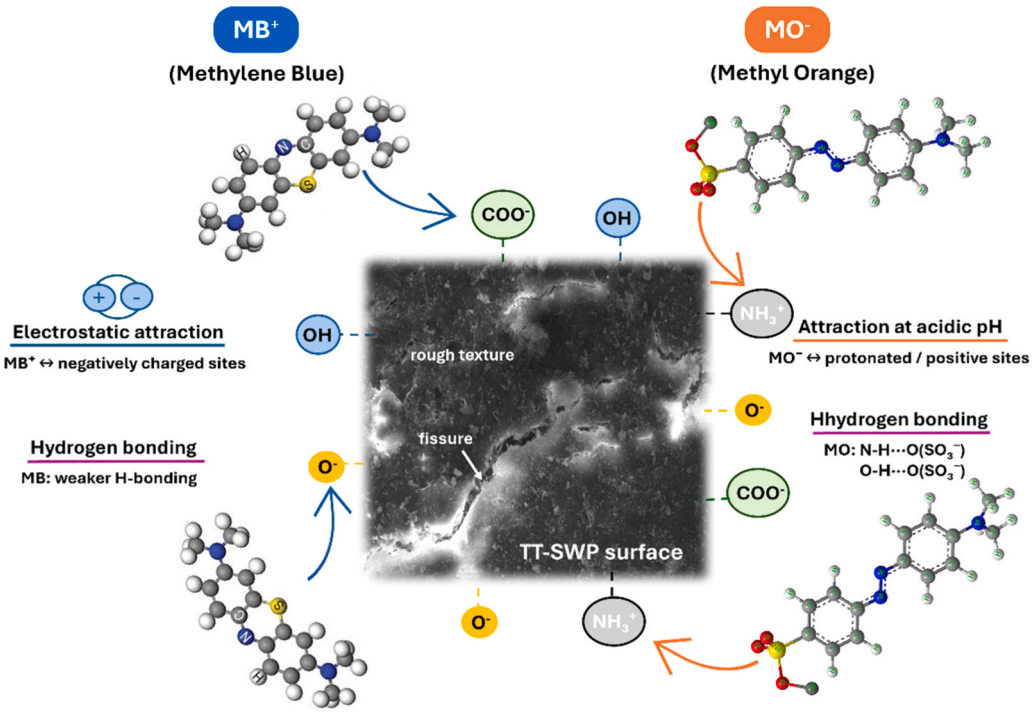

Scheme 2. Proposal adsorption mechanism of MB and MO on SW derived sorbents, illustrated using TT-SWP.

SWP, confirming that TT-SWP sustains higher loadings over much of the concentration range. The corresponding k_L values (≈ 0.0086 −0.049 L mg^{-1}) indicate stronger apparent affinity for MO than for MB on both substrates.

These findings are coherent with the effect of mild thermal treatment on the SWP matrix. Rather than introducing a fundamentally different adsorption pathway, thermal treatment appears to modify the surface morphology and accessibility of adsorption sites, as qualitatively suggested by the rougher and more fissured surface observed by SEM. The better performance of the Langmuir model relative to the Freundlich model at higher C_e suggests that, although some degree of energetic heterogeneity may be present, the dominant adsorption regime remains consistent with monolayer coverage on a finite number of sites [45]. In practical terms, $Q_m$captures the limiting capacity under the tested conditions, whereas $k_L$reflects the affinity/steepness of the isotherm at low C_e; thus, the larger $k_L$values for MO explain the steeper initial rise and the tighter correspondence of the Langmuir curve with the MO data. The Sips model also provided competitive fits for some systems, indicating that limited heterogeneity may exist. However, for TT-SWP-MB, the Sips model yielded Q_m ≈177.06 mg g^{-1} and n = 0.6589, whereas the Langmuir model gave Q_m ≈94.18 mg g^{-1}; given that the experimental isotherm approaches a much lower plateau, the Sips parameters likely reflect overfitting rather than a physically realistic adsorption capacity. By contrast, the Freundlich model, which does not impose a saturation limit, showed larger deviations as C_e approached the plateau region, consistent with its lower R^2 values in Table 5 and its weaker representation of the high-concentration behavior. Overall, the combined evidence from the approach to saturation, the generally better Langmuir fits, and the more cautious interpretation of the Sips parameters supports a predominantly monolayer adsorption mechanism with limited surface heterogeneity.

3.2.6. Adsorption mechanism on TT-SWP surface

Scheme 2 illustrates the proposed adsorption mechanism for MB and MO on SW derived sorbents. Since both SWP and TT-SWP exhibited the same general adsorption trends, differing mainly in magnitude, the mechanistic interpretation is centered on TT-SWP, in which these effects were more clearly expressed. For MB, adsorption is favored at neutral to alkaline pH, where the surface becomes more negatively charged and electrostatic attraction toward the cationic dye is strengthened, with possible secondary contributions from hydrogen bonding and other weak interactions [48]. For MO, adsorption is favored under acidic conditions, where protonated surface groups enhance attraction toward the anionic dye, again with possible additional stabilization through weak intermolecular interactions. The rougher and more fissured surface of TT-SWP is consistent with improved accessibility of adsorption sites. Overall, the results indicate that both dyes are adsorbed through the same general mechanism on SWP and TT-SWP, while thermal treatment enhances the expression of these interactions rather than introducing a fundamentally different adsorption pathway [6].

3.2.7. Comparison of SWP and TT-SWP with other bio-sorbents in retaining MB and MO

The adsorption capacities of various bio-adsorbents for MB and MO, as compiled in Table 6, were reviewed. Comparing the adsorption capacities of SWP and TT-SWP with those reported in the literature reveals that SWP and TT-SWP demonstrate superior effectiveness as adsorbents for MB and MO. Hence, they represent promising low-cost alternatives to other materials for the efficient removal of these dyes. However, it should be emphasized that the adsorption capacities reported in this table depend strongly on the experimental conditions used in each study, including pH, temperature, initial dye concentration, contact time, and adsorbent dosage. Therefore, the comparison should be interpreted with caution and regarded as indicative rather than absolute.

From a comparative perspective, the main strengths of the present study lie in the use of an abundant shrimp-processing residue, the adoption of a simple and reagent-free mild thermal-treatment strategy, and the direct evaluation of untreated and thermally treated sorbents toward both cationic and anionic model dyes. These aspects give the work practical relevance beyond adsorption capacity alone. At the same time, the literature comparison should be interpreted within the limits of the present experimental design, since the study was restricted to two model dyes under batch conditions, only one thermal-treatment

Table 6
Adsorptive capacity of low lost bio-adsorbents for MB and MO dyes.

MB			MO		
Adsorbent	**q_e (mg g^{-1})**	**References**	**Adsorbent**	**q_e (mg g^{-1})**	**References**
Palm bark	2.66	[49]	chitosan-modified biochar	38.75	[50]
Eucalyptus	2.06	[49]	Rice husk-derived biochar	31.63	[50]
Anaerobic digestion residue	9.50	[49]	modified wheat straw	50.4	[51]
Carrot leaves powder	4.35	[52]	aminated pumpkin seed powder	114	[4]
Carrot stem powder	4.10	[52]			
Scenedesmus dimorphus	6.00	[53]	Coffee waste	62.5	[54]
Potato leaves powder	4.25	[55]	Coffee waste	58.82	[54]
Potato stem powder	3.95	[55]	Chicken manure	41.49	[56]
Luffa Actangula Carbon	10.32	[57]	Shaddock peels	94.59	[58]
Carica papaya wood	32.25	[59]	Pomelo peel waste	141.06	[60]
hawthorn kernel	27.34	[61]	Langsat (*Lansium domesticum*) Shell	3.8425	[62]
hawthorn-based bio-adsorbent having sulphonic acid groups	49.99	[61]	*Fucus vesiculosus*	60	[63]
Coconut fibre	29.50	[64]	Typha latifolia pure	36	[65]
Langsat Shell	36.73	[62]	Activated Typha latifolia	50.34	[65]
SWP	65.58	**This study**	SWP	90.15	**This study**
TT-SWP	80.11	**This study**	TT-SWP	98.61	**This study**

protocol was examined, and no BET surface-area analysis was available. Therefore, the present results provide proof-of-concept evidence for a simple and potentially scalable sorbent-upgrading strategy, rather than a definitive benchmark across all pollutant classes or operating conditions.

3.3. Desorption and regeneration study

The desorption behavior of MB and MO adsorbed onto SWP and TT-SWP was evaluated using HCl solutions with concentrations ranging from 0.1 to 0.6 mol L^{-1}. After the adsorption step, the dye-loaded sorbents were separated by centrifugation and then contacted with the eluent under stirring for 90 min to promote dye desorption. Following desorption, the recovered sorbents were washed three times with 60 mL of 50% ethanol for 60 min in order to remove residual dye and acid, and were then reused in the subsequent adsorption cycle [45]. The desorption efficiency was calculated from the ratio between the amount of dye released into the eluent and the amount previously adsorbed onto the sorbent. The desorption results showed that dye release depended strongly on both the sorbent type and the acid concentration (Figs. 8**a** and 8**b**). For SWP, MO exhibited markedly higher desorption than MB at low HCl concentrations, reaching its highest value at 0.1 mol L^{-1}, whereas MB desorption increased progressively and reached a maximum at intermediate acid concentration before decreasing again at higher HCl concentrations. A similar concentration-dependent behavior was also observed for TT-SWP, although the relative trends of the two dyes differed. In general, MO was more easily desorbed than MB at low acid concentration, while MB desorption became more pronounced at intermediate HCl concentrations. These results indicate that the reversibility of adsorption was strongly affected by dye type and by the interaction strength established with the sorbent surface. They also suggest that improved adsorption performance does not necessarily correspond to higher desorption efficiency under the same regeneration conditions.

The regeneration study further showed that both SWP and TT-SWP remained reusable over five consecutive adsorption-desorption cycles, although a progressive decline in removal efficiency was observed in all cases (Fig. 8**c** and **d**). For MB, SWP retained higher removal efficiency than TT-SWP throughout the investigated cycles, indicating better regeneration stability under the selected conditions. For MO, TT-SWP showed higher removal efficiency than SWP during the first cycles, confirming its superior initial adsorption performance, although the difference between the two sorbents became smaller at later cycles. The gradual decrease in removal efficiency for both dyes suggests partial regeneration of the active sites and progressive loss of adsorption capacity upon repeated use, likely due to incomplete dye desorption and/or partial blocking of adsorption sites.

Overall, these results confirm that regeneration of SWP and TT-SWP is feasible, but also show that cyclic stability remains moderate rather than complete under the present conditions. From a practical perspective, the regeneration behavior supports the potential reuse of both sorbents, while indicating that further optimization of the regeneration medium and operating conditions would be required to improve long-term performance.

4. Conclusions

This study demonstrated that SWP and its thermally treated derivative at 200 °C can serve as effective and low-cost biosorbents for the removal of MB and MO from aqueous solutions. Thermal treatment induced significant modifications in surface morphology and properties, leading to enhanced adsorption performance, particularly for MO. The experimental data were well described by the Langmuir isotherm model and a PSO kinetic model. Thermodynamic analysis revealed an endothermic process for MB adsorption and an exothermic one for MO, with physical interactions predominating in both cases. In addition, regeneration tests indicated moderate reusability of the materials over several adsorption-desorption cycles. The main advantage of this work lies in the use of a simple, reagent-free thermal treatment applied to an abundant by-product, making this approach sustainable and potentially scalable for industrial applications. However, this study has some limitations, including the use of batch experimental conditions and a limited number of model pollutants. Future work should therefore focus on continuous-flow system investigations, evaluation using real industrial effluents, and extension to other classes of contaminants such as heavy metals, pesticides, and other organic pollutants. Furthermore, exploring different thermal treatment conditions and alternative treatment methods, as well as conducting additional surface characterization analyses such as Transmission electron microscopy, X-ray photoelectron spectroscopy, and Brunauer-Emmett-Teller, would provide deeper insight into the adsorption mechanisms. In this context, the present findings provide a promising proof of concept for the development of low-cost biosorbents for sustainable water treatment.

CRediT authorship contribution statement

Mohamed Achache: Conceptualization, Formal analysis, Writing – original draft, Writing – review & editing. **Santa Olga Cacciola:** Supervision, Writing – review & editing. **Abderrahmane Debdoubi:**

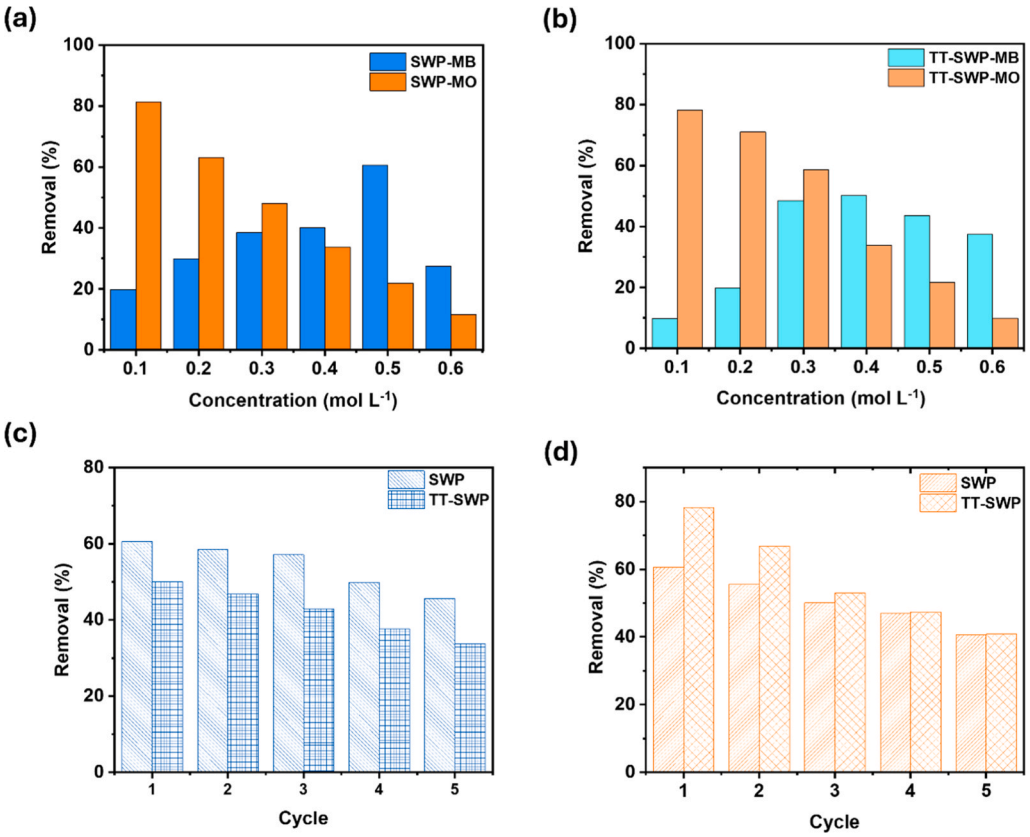

Fig. 8. Desorption of MB and MO from SWP (a) and TT-SWP (b) using HCl solutions of different concentrations, and regeneration performance of SWP and TT-SWP over five adsorption-desorption cycles for MB (c) and MO (d).

Supervision, Writing – review & editing. **Soumia El Boumlasy:** Conceptualization, Formal analysis, Investigation, Methodology, Writing – original draft, Writing – review & editing. **Iman Kouda:** Conceptualization, Methodology, Visualization, Writing – review & editing. **Federico La Spada:** Writing – original draft, Writing – review & editing. **Nunzio Tuccitto:** Writing – original draft, Writing – review & editing.

Consent to publish declaration

Not applicable.

Ethics approval and consent to participate

Not Applicable.

Funding

No funding.

Declaration of Competing Interest

The authors declare that they have no known competing financial interests or personal relationships that could have appeared to influence the work reported in this paper.

Data availability

All analysed data where been included in this respective published article. Raw data can be shared upon reasonable request.

References

[1] T.K. Saha, N.C. Bhoumik, S. Karmaker, M.G. Ahmed, H. Ichikawa, Y. Fukumori, Adsorption of methyl orange onto chitosan from aqueous solution, Art. no. 10, JWARP 02 (10) (2010), https://doi.org/10.4236/jwarp.2010.210107.
[2] R. Al-Tohamy, et al., A critical review on the treatment of dye-containing wastewater: Ecotoxicological and health concerns of textile dyes and possible remediation approaches for environmental safety, Ecotoxicol. Environ. Saf. 231 (Feb. 2022) 113160, https://doi.org/10.1016/j.ecoenv.2021.113160.
[3] S. Hussain, et al., Adsorption, kinetics and thermodynamics studies of methyl orange dye sequestration through chitosan composites films, Int. J. Biol. Macromol. 168 (Jan. 2021) 383–394, https://doi.org/10.1016/j.ijbiomac.2020.12.054.
[4] M.V. Subbaiah, D.-S. Kim, Adsorption of methyl orange from aqueous solution by aminated pumpkin seed powder: kinetics, isotherms, and thermodynamic studies, Ecotoxicol. Environ. Saf. 128 (Jun. 2016) 109–117, https://doi.org/10.1016/j.ecoenv.2016.02.016.
[5] E. Errais, et al., Efficient anionic dye adsorption on natural untreated clay: kinetic study and thermodynamic parameters, Art. no. 1–3, Desalination 275 (1–3) (Jul. 2011), https://doi.org/10.1016/j.desal.2011.02.031.
[6] K.O. Iwuozor, J.O. Ighalo, E.C. Emenike, L.A. Ogunfowora, C.A. Igwegbe, Adsorption of methyl orange: a review on adsorbent performance, Curr. Res. Green. Sustain. Chem. 4 (Jan. 2021) 100179, https://doi.org/10.1016/j.crgsc.2021.100179.
[7] D.T. Huong, N.N.P. Ngan, D.T.T. Anh, N.D. Vinh, V.T. Xuan, Durian peel–seed biochar for efficient methylene blue removal from water: synthesis, characterization, and adsorption performance, RSC Adv. 15 (40) (Sep. 2025) 33726–33749, https://doi.org/10.1039/D5RA05313G.
[8] K. Yamsomphong, et al., Excellent but strange adsorption performance of shrimp shell-derived adsorbent for anionic pollutant removal, Chem. Eng. J. 515 (Jul. 2025) 163683, https://doi.org/10.1016/j.cej.2025.163683.
[9] P. Kumar, et al., A critical review on recent developments in the low-cost adsorption of dyes from wastewater, Desalination Water Treat. 172 (Jan. 2019) 395–416, https://doi.org/10.5004/dwt.2019.24613.
[10] K.S. Bharathi, S.T. Ramesh, Removal of dyes using agricultural waste as low-cost adsorbents: a review, Art. no. 4, Appl. Water Sci. 3 (4) (Dec. 2013), https://doi.org/10.1007/s13201-013-0117-y.
[11] G. Kataya, et al., Dynamic removal of methylene blue and methyl orange from water using biochar derived from kitchen waste, Sci. Rep. 15 (1) (Aug. 2025) 29907, https://doi.org/10.1038/s41598-025-14133-6.
[12] P.C. R. M, S. T, V. G, Efficient adsorption of methyl orange dye by novel chitosan-biochar hybrid zinc oxide composites, Biomass. Conv. Bioref. 15 (11) (Jun. 2025) 17267–17293, https://doi.org/10.1007/s13399-025-06856-3.

[13] G. Zheng, P. Fu, X. Li, Frontiers in machine learning strategies for dye removal in water treatment, J. Water Process Eng. 71 (Mar. 2025) 107251, https://doi.org/10.1016/j.jwpe.2025.107251.
[14] M.M. Kwikima, S. Mateso, Y. Chebude, Potentials of agricultural wastes as the ultimate alternative adsorbent for cadmium removal from wastewater. A review, Sci. Afr. 13 (Sep. 2021) e00934, https://doi.org/10.1016/j.sciaf.2021.e00934.
[15] M. Achache, et al., Innovative use of shrimp shell powder in carbon paste electrode for the electrochemical detection of dopamine and paracetamol: Valorization, characterization and application, Microchem. J. 202 (Jul. 2024) 110754, https://doi.org/10.1016/j.microc.2024.110754.
[16] S. El Boumlasy, D. Mangraviti, K. Arena, F. Cacciola, F. Asraoui, A. Debdoubi, Determination of astaxanthin and astaxanthin esters in three samples of shrimp waste (Parapenaeus longirostris) by high performance liquid chromatography coupled photo-diode array and mass spectrometry detection, Nat. Prod. Res. (Aug. 2023), https://doi.org/10.1080/14786419.2023.2245959.
[17] N. Rossi, C. Grosso, C. Delerue-Matos, Shrimp waste upcycling: unveiling the potential of polysaccharides, proteins, carotenoids, and fatty acids with emphasis on extraction techniques and bioactive properties, Art. no. 4, Mar. Drugs 22 (4) (Apr. 2024), https://doi.org/10.3390/md22040153.
[18] E. Atangana, T.O. Ajiboye, A.A. Mafolasire, S. Ghosh, B. Hakeem, Adsorption of organic pollutants from wastewater using chitosan-based adsorbents, Polymers 17 (4) (Jan. 2025) 502, https://doi.org/10.3390/polym17040502.
[19] T. Bahadir, G. Gök, H. Çelebi, İ. Şimşek, O. Gök, Seafood wastes as an attractive biosorbent: chitin-based shrimp shells, Water Air Soil Pollut. 234 (3) (Feb. 2023) 145, https://doi.org/10.1007/s11270-023-06167-1.
[20] S. El boumlasy, et al., Inhibitory activity of shrimp waste extracts on fungal and oomycete plant pathogens, Art. no. 11, Plants 10 (11) (Nov. 2021), https://doi.org/10.3390/plants10112452.
[21] I. Kouda, et al., Enhanced cationic dyes adsorption: experimental and theoretical insights into Moroccan clays vs. commercial montmorillonite, Surf. Interfaces 59 (Feb. 2025) 105946, https://doi.org/10.1016/j.surfin.2025.105946.
[22] L. Luo, et al., Synthesis of activated carbon from biowaste of fir bark for methylene blue removal, Art. no. 9, R. Soc. Open Sci. 6 (9) (Sep. 2019), https://doi.org/10.1098/rsos.190523.
[23] S. Bakhta, Z. Sadaoui, N. Boudechiche, H. Hafsa, K. Sellami, J. Vieillard, Eco-friendly adsorption of a cationic dye using a chemically modified industrial by-product: process optimization and modeling, RSC Adv. 15 (46) (2025) 38435–38453, https://doi.org/10.1039/D5RA05466D.
[24] H. Kim, S.-O. Kang, S. Park, H.S. Park, Adsorption isotherms and kinetics of cationic and anionic dyes on three-dimensional reduced graphene oxide macrostructure, J. Ind. Eng. Chem. 21 (Jan. 2015) 1191–1196, https://doi.org/10.1016/j.jiec.2014.05.033.
[25] Z. Alasmary, M.A. Akanji, Iron-modified biochar derived from poultry manure for efficient removal of methyl orange dye from aqueous solution, Sustainability 17 (13) (Jan. 2025) 6008, https://doi.org/10.3390/su17136008.
[26] I. Kouda, N. Ben Seddik, A. Laaziz, M. Hadri, K. Draoui, A. Elmidaoui, Efficient removal of cationic dye from wastewater using novel low-cost adsorbent, cellulose-clay composite: insights from isotherm, kinetic, thermodynamic, and molecular dynamics simulation studies, J. Mol. Struct. 1291 (Nov. 2023) 135865, https://doi.org/10.1016/j.molstruc.2023.135865.
[27] O.P. Gbenebor, S.O. Adeosun, G.I. Lawal, S. Jun, S.A. Olaleye, Acetylation, crystalline and morphological properties of structural polysaccharide from shrimp exoskeleton, Eng. Sci. Technol. Int. J. 20 (3) (Jun. 2017) 1155–1165, https://doi.org/10.1016/j.jestch.2017.05.002.
[28] G. Mujtaba, et al., Potential of Capparis decidua plant and eggshell composite adsorbent for effective removal of anionic dyes from aqueous medium, Environ. Res. 247 (Apr. 2024) 118279, https://doi.org/10.1016/j.envres.2024.118279.
[29] H.A. Omar, H.Y. Katman, M. Bilema, M.K.A. Ahmed, A. Milad, N.I. Md Yusoff, The effect of ageing on chemical and strength characteristics of nanoclay-modified bitumen and asphalt mixture, Art. no. 15, Appl. Sci. 11 (15) (Jan. 2021), https://doi.org/10.3390/app11156709.
[30] A. Segalina, et al., Cocrystals of nitrofurantoin: how coformers can modify its solubility and permeability across intestinal cell monolayers, Cryst. Growth & Des. 22 (5) (May 2022) 3090–3106, https://doi.org/10.1021/acs.cgd.2c00007.
[31] J. Milošević, R. Prodanović, N. Polović, On the protein fibrillation pathway: oligomer intermediates detection using ATR-FTIR spectroscopy, Art. no. 4, Molecules 26 (4) (Jan. 2021), https://doi.org/10.3390/molecules26040970.
[32] J.A. Asong, E.K. Frimpong, H.A. Seepe, L. Katata-Seru, S.O. Amoo, A.O. Aremu, Green synthesis of characterized silver nanoparticle using cullen tomentosum and assessment of its antibacterial activity, Art. no. 2, Antibiotics 12 (2) (Feb. 2023), https://doi.org/10.3390/antibiotics12020203.
[33] W.D. Pita Rengga, K.A. Salsabiil, Harianingsih, S.E. Oktavia, M. Ansori, Flavored powder from shrimp shells with bromelain enzymatic process and adding of flour and spices, J. Phys. Conf. Ser. 1367 (1) (Nov. 2019) 012080, https://doi.org/10.1088/1742-6596/1367/1/012080.
[34] A. Lourenço, et al., Valorisation of lignocellulosic wastes, the case study of eucalypt stumps lignin as bioadsorbent for the removal of Cr(VI), Art. no. 19, Molecules 27 (19) (Jan. 2022), https://doi.org/10.3390/molecules27196246.
[35] S. Liu, et al., Effects of biochar pyrolysis temperature on thermal properties of polyethylene glycol/biochar composites as shape-stable biocomposite phase change materials, RSC Adv. 12 (16) (2022) 9587–9598, https://doi.org/10.1039/D1RA09167K.
[36] M. Achache, S. El Boumlasy, D. Bouchta, M. Choukairi, Development and applications of carbon paste and Sonogel-Carbon electrodes modified with nanomaterials: perspectives in pharmaceutical, biological, environmental and food analysis: a review, TrAC Trends Anal. Chem. 194 (Jan. 2026) 118502, https://doi.org/10.1016/j.trac.2025.118502.
[37] R. Shabir, Y. Li, M. Megharaj, C. Chen, Pyrolysis temperature affects biochar suitability as an alternative rhizobial carrier, Biol. Fertil. Soils 60 (5) (Jul. 2024) 681–697, https://doi.org/10.1007/s00374-024-01805-0.
[38] Y. Aoulad El Hadj Ali, M. Ahrouch, A. Ait Lahcen, A. Demba N'diaye, F. El Yousfi, M. Stitou, Dried sewage sludge as an efficient adsorbent for pollutants: cationic methylene blue removal case study, Art. no. 1, Nanotechnol. Environ. Eng. 6 (1) (May 2021), https://doi.org/10.1007/s41204-021-00111-6.
[39] I. Ayouch, et al., Crosslinked carboxymethyl cellulose-hydroxyethyl cellulose hydrogel films for adsorption of cadmium and methylene blue from aqueous solutions, Surf. Interfaces 24 (Jun. 2021) 101124, https://doi.org/10.1016/j.surfin.2021.101124.
[40] E. Rápó, S. Tonk, Factors affecting synthetic dye adsorption; desorption studies: a review of results from the last five years (2017–2021), Art. no. 17, Molecules 26 (17) (Jan. 2021), https://doi.org/10.3390/molecules26175419.
[41] I. Kouda, et al., Impact of solvent treatment on the adsorption efficiency of crystal violet dye using cellulose acetate-clay composite membranes: experimental and molecular dynamics approaches, Carbohydr. Polym. 357 (Jun. 2025) 123494, https://doi.org/10.1016/j.carbpol.2025.123494.
[42] D. Morantes, E. Muñoz, D. Kam, O. Shoseyov, Highly charged cellulose nanocrystals applied as a water treatment flocculant, Art. no. 2, Nanomaterials 9 (2) (Feb. 2019), https://doi.org/10.3390/nano9020272.
[43] M. Zaman, H. Xiao, F. Chibante, Y. Ni, Synthesis and characterization of cationically modified nanocrystalline cellulose, Carbohydr. Polym. 89 (1) (Jun. 2012) 163–170, https://doi.org/10.1016/j.carbpol.2012.02.066.
[44] S. Banerjee, S. Dubey, R.K. Gautam, M.C. Chattopadhyaya, Y.C. Sharma, Adsorption characteristics of alumina nanoparticles for the removal of hazardous dye, Orange G from aqueous solutions, Arab J. Chem. 12 (8) (Dec. 2019) 5339–5354, https://doi.org/10.1016/j.arabjc.2016.12.016.
[45] F.M. Mohamed, et al., Sustainable removal of azo dyes from real effluents using a biomass-derived composite, Sci. Rep. 16 (1) (Jan. 2026) 2076, https://doi.org/10.1038/s41598-025-32434-8.
[46] Y. Yu, Y.-Y. Zhuang, Z.-H. Wang, Adsorption of water-soluble dye onto functionalized resin, J. Colloid Interface Sci. 242 (2) (Oct. 2001) 288–293, https://doi.org/10.1006/jcis.2001.7780.
[47] P. Saha, S. Chowdhury, Insight into adsorption thermodynamics, in: M. Tadashi (Ed.), Thermodynamics, InTech, 2011, https://doi.org/10.5772/13474.
[48] S.T. Al-Asadi, et al., A comprehensive review of methylene blue dye adsorption on activated carbon from edible fruit seeds: a case study on kinetics and adsorption models, Carbon Trends 20 (Aug. 2025) 100507, https://doi.org/10.1016/j.cartre.2025.100507.
[49] L. Sun, S. Wan, W. Luo, Biochars prepared from anaerobic digestion residue, palm bark, and eucalyptus for adsorption of cationic methylene blue dye: characterization, equilibrium, and kinetic studies, Bioresour. Technol. 140 (Jul. 2013) 406–413, https://doi.org/10.1016/j.biortech.2013.04.116.
[50] J.-H. Huang, K.-L. Huang, S.-Q. Liu, A.-T. Wang, C. Yan, Adsorption of Rhodamine B and methyl orange on a hypercrosslinked polymeric adsorbent in aqueous solution, Art. no. 1, Colloids Surf. A Physicochem. Eng. Asp. 330 (1) (Nov. 2008), https://doi.org/10.1016/j.colsurfa.2008.07.050.
[51] Y. Su, Y. Jiao, C. Dou, R. Han, Biosorption of methyl orange from aqueous solutions using cationic surfactant-modified wheat straw in batch mode, Desalin. Water Treat. 52 (31) (Sep. 2014) 6445–6455, https://doi.org/10.1080/19443994.2013.811121.
[52] A.K. Kushwaha, N. Gupta, M.C. Chattopadhyaya, Removal of cationic methylene blue and malachite green dyes from aqueous solution by waste materials of Daucus carota, Art. no. 3, J. Saudi Chem. Soc. 18 (3) (Jul. 2014), https://doi.org/10.1016/j.jscs.2011.06.011.
[53] T. Sarat Chandra, et al., Defatted algal biomass as a non-conventional low-cost adsorbent: surface characterization and methylene blue adsorption characteristics, Bioresour. Technol. 184 (May 2015) 395–404, https://doi.org/10.1016/j.biortech.2014.10.018.
[54] R. Lafi, A. Hafiane, Removal of methyl orange (MO) from aqueous solution using cationic surfactants modified coffee waste (MCWs), J. Taiwan Inst. Chem. Eng. 58 (Jan. 2016) 424–433, https://doi.org/10.1016/j.jtice.2015.06.035.
[55] N. Gupta, A.K. Kushwaha, M.C. Chattopadhyaya, Application of potato (Solanum tuberosum) plant wastes for the removal of methylene blue and malachite green dye from aqueous solution, Arab. J. Chem. 9 (Sep. 2016) S707–S716, https://doi.org/10.1016/j.arabjc.2011.07.021.
[56] J. Yu, X. Zhang, D. Wang, P. Li, Adsorption of methyl orange dye onto biochar adsorbent prepared from chicken manure, Art. no. 5, Water Sci. Technol. 77 (5) (Jan. 2018), https://doi.org/10.2166/wst.2018.003.
[57] S.H. Siddiqui, The removal of Cu^{2+}, Ni^{2+} and Methylene Blue (MB) from aqueous solution using Luffa Actangula Carbon: kinetics, thermodynamic and isotherm and response methodology, Groundw. Sustain. Dev. 6 (Mar. 2018) 141–149, https://doi.org/10.1016/j.gsd.2017.12.008.
[58] X. Tao, Y. Wu, L. Cha, Shaddock peels-based activated carbon as cost-saving adsorbents for efficient removal of Cr (VI) and methyl orange, Art. no. 19, Environ. Sci. Pollut. Res 26 (19) (Jul. 2019), https://doi.org/10.1007/s11356-019-05322-8.
[59] R.S. S. Lata, B. P, Biosorption characteristics of methylene blue and malachite green from simulated wastewater onto Carica papaya wood biosorbent, Surf. Interfaces 10 (Mar. 2018) 197–215, https://doi.org/10.1016/j.surfin.2017.09.011.
[60] B. Zhang, Y. Wu, L. Cha, Removal of methyl orange dye using activated biochar derived from pomelo peel wastes: performance, isotherm, and kinetic studies, Art. no. 1, J. Dispers. Sci. Technol. 41 (1) (Jan. 2020), https://doi.org/10.1080/01932691.2018.1561298.

[61] Y. Akköz, R. Coşkun, A. Delibaş, Preparation and characterization of sulphonated bio-adsorbent from waste hawthorn kernel for dye (MB) removal, J. Mol. Liq. 287 (Aug. 2019) 110988, https://doi.org/10.1016/j.molliq.2019.110988.
[62] D. Kurniawati, Bahrizal, T.K. Sari, F. Adella, S. Sy, Effect of contact time adsorption of rhodamine B, methyl orange and methylene blue colours on langsat shell with batch methods, Art. no. 1, J. Phys. Conf. Ser. 1788 (1) (Feb. 2021), https://doi.org/10.1088/1742-6596/1788/1/012008.
[63] N.E.-A. El-Naggar, R.A. Hamouda, A.A. Saddiq, M.H. Alkinani, Simultaneous bioremediation of cationic copper ions and anionic methyl orange azo dye by brown marine alga Fucus vesiculosus, Art. no. 1, Sci. Rep. 11 (1) (Feb. 2021), https://doi.org/10.1038/s41598-021-82827-8.
[64] C.E.D.F. Silva, B.M.V.D. Gama, A.H.D.S. Gonçalves, J.A. Medeiros, A.K.D.S. Abud, Basic-dye adsorption in albedo residue: effect of pH, contact time, temperature, dye concentration, biomass dosage, rotation and ionic strength, Art. no. 6, J. King Saud. Univ. Eng. Sci. 32 (6) (Sep. 2020), https://doi.org/10.1016/j.jksues.2019.04.006.
[65] A. El Amri, et al., Investigation of Typha latifolia (TL) as potential biosorbent for removal of the methyl orange anionic dye in the aqueous solution. Kinetic and DFT approaches, J. Mol. Struct. 1272 (Jan. 2023) 134098, https://doi.org/10.1016/j.molstruc.2022.134098.